Materials Research Express

PAPER • OPEN ACCESS

Magnetocaloric effect and critical behavior near the first to second-order phase transition of $La_{0.7}Ca_{0.3-x}Sn_xMnO_3$ compounds

To cite this article: Dao Son Lam *et al* 2020 *Mater. Res. Express* **7** 046101

Materials Research Express

OPEN ACCESS

RECEIVED
9 February 2020

REVISED
20 March 2020

ACCEPTED FOR PUBLICATION
30 March 2020

PUBLISHED
13 April 2020

PAPER

Magnetocaloric effect and critical behavior near the first to second-order phase transition of $La_{0.7}Ca_{0.3-x}Sn_xMnO_3$ compounds

Dao Son Lam[1], Nguyen Thi Dung[1,2,3,6], Tran Dang Thanh[1,2,6], Dinh Chi Linh[1,2], Wen-Zhe Nan[4] and Seong Cho Yu[4,5]

[1] Institute of Materials Science, Vietnam Academy of Science and Technology, 18-Hoang Quoc Viet, Hanoi, Vietnam
[2] Graduate University of Science and Technology, Vietnam Academy of Science and Technology, 18-Hoang Quoc Viet, Hanoi, Vietnam
[3] Thai Nguyen University of Science - Thai Nguyen University, Thai Nguyen, Vietnam
[4] Department of Physics, Chungbuk National University, Cheongju 28644, Republic of Korea
[5] Ulsan National Institute of Science and Technology, Ulsan 44919, Republic of Korea
[6] Authors to whom any correspondence should be addressed.

E-mail: dung.nt@tnus.edu.vn **and** thanhxraylab@yahoo.com

Keywords: magnetocaloric effect, critical behavior, ferromagnetic interactions

Abstract

The magnetocaloric effect and the critical behavior near the first to second-order phase transition of $La_{0.7}Ca_{0.3-x}Sn_xMnO_3$ compounds (with $x = 0$–0.04), which were prepared by a conventional solid state reaction method, have been investigated. With increasing Sn-doping, a systematic decrease in the Curie temperature (T_C) and the magnetic entropy change (ΔS_m) are observed. We also pointed out that the width and the order of the magnetic phase transition in $La_{0.7}Ca_{0.3-x}Sn_xMnO_3$ compounds can be easily modified by changing Sn concentration. The Banerjee criterion suggests that the Sn-undoped sample ($x = 0$) undergoes a first-order phase transition (FOPT). Meanwhile, Sn-doped samples ($x = 0.02$ and 0.04) undergo a second-order phase transition (SOPT). Based on the Kouvel-Fisher method and the critical isotherm analyses, we have determined the values of the critical exponents (β, γ, and δ) and T_C for two SOPT samples. The results obtained for $x = 0.02$ sample are $\beta = 0.218$, $\gamma = 0.858$, and $\delta = 4.717$, which are close to those expected for the tricritical mean field theory. Whereas, $\beta = 0.468$, $\gamma = 1.095$ and $\delta = 3.315$ obtained for $x = 0.04$ sample are close to those expected for the mean field theory. This suggests that the presence of Sn favors establishing the ferromagnetic long-range interactions in the sample.

1. Introduction

It is known that the hole doped perovskite manganite $La_{0.7}Ca_{0.3}MnO_3$ is a typical material exhibiting a colossal magnetoresistance (CMR) and a magnetocaloric effect (MCE) with high values magnetoresistance (MR) and magnetic entropy change (ΔS_m), respectively. These values are almost larger than those obtained on the other manganites [1–7]. Nevertheless, $La_{0.7}Ca_{0.3}MnO_3$ polycrystalline or single crystal bulk sample is a first-order phase transition (FOPT) material [8–11]. There are two important drawbacks in the FOPT materials, namely the narrowness of the FM-PM phase transition region and the presence of the thermal and magnetic hysteresis, which limit their applicability [12]. To improve these drawbacks, it is necessary to modify the order of phase transition in $La_{0.7}Ca_{0.3}MnO_3$ compound from FOPT to SOPT.

Recent studies have shown that there are some ways to modify the order of phase transition in $La_{0.7}Ca_{0.3}MnO_3$ compound, including reduced dimensionality [11], reduced crystalline or particle size [9, 13], and doped suitable elements into the La/Ca [14–18] and/or Mn sites [19, 20]. Depending on crystalline size, dopant types, and doping content, modifying the FOPT to SOPT results would be different. To distinguish whether a material is the FOPT or SOPT, we can use the criteria proposed by Banerjee [21]. According to these criteria, H/M is plotted versus M^2 in the vicinity of T_C. A material is a FOPT if there is a negative slope on some H/M versus M^2 curves, while a positive slope corresponds to a SOPT [21]. Besides, it is known that the β, γ, and δ

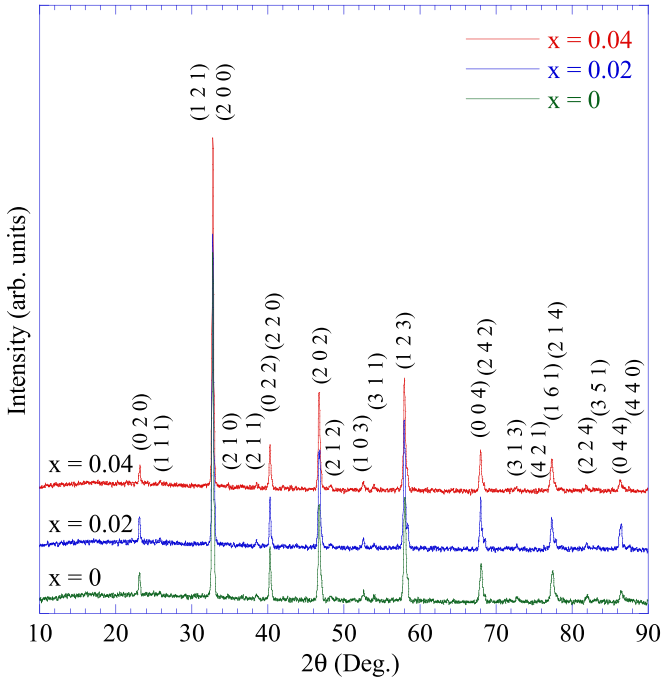

Figure 1. XRD patterns of $La_{0.7}Ca_{0.3-x}Sn_xMnO_3$ compounds.

critical exponents which featured for the SOPT around T_C are corresponded with the M_S spontaneous magnetization, the χ_0^{-1} magnetic susceptibility at the beginning, the critical isotherm at T_C [22, 23].

To further understand the MCE and the critical behaviors near the first to second-order phase transition, we prepared three samples of $La_{0.7}Ca_{0.3-x}Sn_xMnO_3$ (with $x = 0.0$, 0.02, and 0.04) and studied their magnetic characters. The dependences of magnetic entropy change on temperature and applied magnetic field were determined by using the Maxwell relation and a phenomenological model [24, 25]. Besides, we applied the Banerjee's criteria [21], the Kouvel-Fisher method [23], and the critical isotherm analyses [22] to investigate the critical behaviors for samples. We pointed out that the presence of Sn favors establishing the SOPT and the FM long-range interactions in $La_{0.7}Ca_{0.3-x}Sn_xMnO_3$ compounds.

2. Experimental details

With the solid-state reaction procedure, we synthesized three bulk samples of $La_{0.7}Ca_{0.3-x}Sn_xMnO_3$ ($x = 0$, 0.02, and 0.04). The precursors are highly immaculate powders (99.9%) of Sigma-Aldrich included La_2O_3, $CaCO_3$, SnO_2, and Mn_3O_4. The mass of these precursors were calculated and weighed according to the nominal composition ($La_{0.7}Ca_{0.3-x}Sn_xMnO_3$), then were crushed, blended, and calcinated at 1200 °C in about 24 h in the air. Thereafter, the mixed products were crushed again, pressed tablets under a pressure of 4000 kg cm^{-2} and sintered at 1400 °C within 28 h in the air. X-ray diffraction (XRD) patterns at room temperature of final products were recorded on an x-ray diffractometer (Equinox 5000, Thermo Scientific) using a Cu-K_α radiation source ($\lambda = 1.5406$ Å). The grain size and the component of samples were estimated through the scanning electronic microscopy (SEM) image and the energy dispersive x-ray (EDX) spectroscopy on a Fe-SEM (S4800, Hitachi). The magnetization depends on temperature and magnetic field was measured on a vibrating sample magnetometer system.

3. Results and discussion

These XRD patterns for samples are presented in figure 1. All XRD peaks in each pattern correspond to the Miller indexes of an orthorhombic structure, *Pnma* space group, and suitable for a PDF card No. 01-089-8075 [26] in the international centre for diffraction data. This confirms that all samples are single phase of $La_{0.7}Ca_{0.3-x}Sn_xMnO_3$, without any secondary phase. The lattice parameters for samples were estimated and showed in table 1. Clearly, the presence of Sn does not change the orthorhombic structure but modifies the value of the lattice parameters. A slight decrease in these parameters with increasing Sn concentration was observed. This could be related to the average ionic radius of A-site ($\langle r_A \rangle$) in perovskite structure ABO_3 [27, 28]. Our result

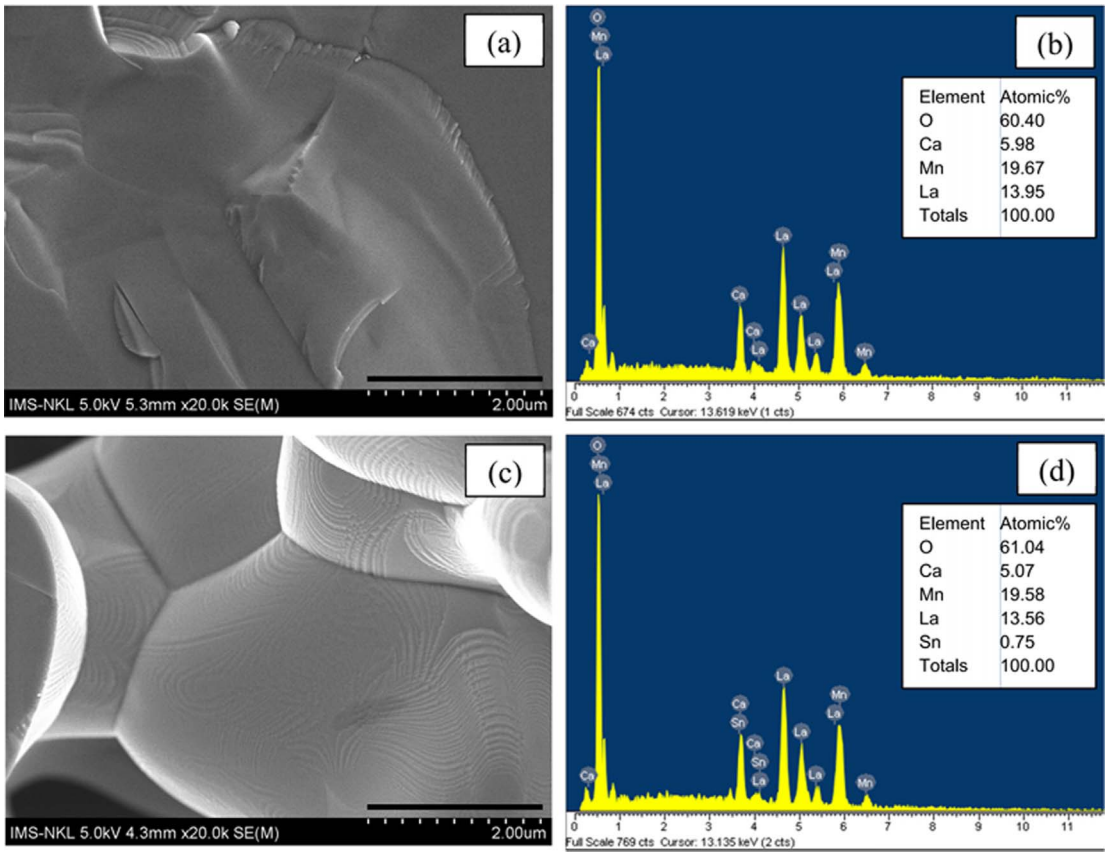

Figure 2. SEM images and EDX spectra for two representatives: (a) and (b) for $x = 0$, (c) and (d) for $x = 0.04$.

Table 1. Lattice parameters of $La_{0.7}Ca_{0.3-x}Sn_xMnO_3$ compounds.

x	$\langle r_A \rangle$ (Å)	a (Å)	b (Å)	c (Å)	V (Å^3)
0	1.354(0)	5.457(1)	7.712(3)	5.474(6)	230.40(8)
0.02	1.350(8)	5.456(4)	7.711(9)	5.474(7)	230.37(1)
0.04	1.347(6)	5.456(1)	7.711(3)	5.473(7)	230.29(8)

is completely opposite when Sn substituted into Mn-site (B-site) in similar manganites [28, 29]. An increase of the unit cell parameters was observed when Sn substituted into Mn-site in $La_{0.67}Ba_{0.33}Mn_{1-x}Sn_xO_3$ [30] and $La_{0.57}Nd_{0.1}Sr_{0.33}Mn_{1-x}Sn_xO_3$ [29] compounds. This result has been explained by the substitution of Sn^{4+} with a larger ionic radius ($r_{Sn4+} = 0.69$ Å) for Mn^{4+} with a smaller radius ($r_{Mn4+} = 0.53$ Å). Therefore, in our work, the substitution of Sn into Mn-site would not have happened.

In order to explain the increase of the lattice parameters of $La_{0.7}Ca_{0.3-x}Sn_xMnO_3$ compounds when increasing the amount of Sn, we have assumed that the valence of Sn ion is 2+ and it could be substituted into A-site because $r_{Sn2+} = 1.18$ Å, which is quite close to that of Ca^{2+} (1.34 Å) or La^{3+} (1.36 Å). Therefore, the average ionic radius of A-site could be deduced as $\langle r_A \rangle = 0.7r_{La3+} + (0.3\text{-}x)r_{Ca2+} + xr_{Sn2+}$. Using the ionic radii $r_{La3+} = 1.36$ Å, $r_{Ca2+} = 1.34$ Å, and $r_{Sn2+} = 1.18$ Å [31], the value of $\langle r_A \rangle$ is found to be 1.354 Å, 1.350 Å, and 1.347 Å for $x = 0$, 0.02, and 0.04, respectively (table 1). It shows that the $\langle r_A \rangle$ value monotonously decreases with increasing Sn concentration. Thus we believe the slight decrease of the unit-cell volume of $La_{0.7}Ca_{0.3-x}Sn_xMnO_3$ is closely related to the substitution of Sn^{2+} with a smaller ionic radius (1.18 Å) for La^{3+}/Ca^{2+} ions (1.36 Å/1.34 Å).

Figure 2 show SEM images and EDX spectra of two samples with $x = 0$ and 0.04. We can see that their grain size reaches about micrometers with sharp grain boundary, figures 2(a) and (c). The EDX spectra show peaks corresponding to lanthanum, calcium, manganese, oxygen, and tin, figures 2(b) and (d). These elements are included in the samples, without any strange elements. The values of atomic percentage obtained are quite close to those expected of compounds. It means that starting materials have fully reacted to create $La_{0.7}Ca_{0.3-x}Sn_xMnO_3$ phase, no element is neither lost nor added during the fabrication process.

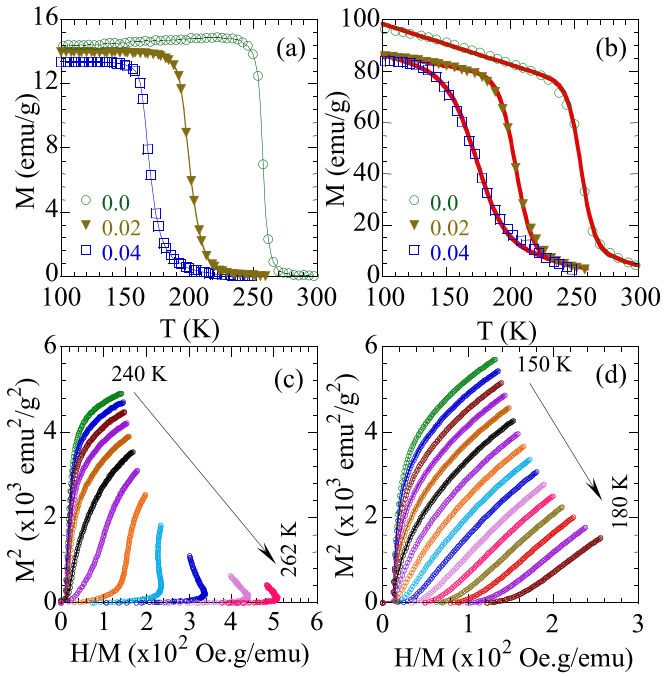

Figure 3. (a) and (b) $M(T)$ curves at $H = 100$ Oe and 10 kOe, respectively. (c) and (d) Arrott plots of M^2 versus H/M curves for two representative samples with $x = 0$ and 0.04, respectively.

Table 2. The fitting parameters of $M(T)$ data to equation (1), and the values of $|\Delta S_{max}|$ and RC calculated to equation (2) for $La_{0.7}Ca_{0.3-x}Sn_xMnO_3$ samples under $\Delta H = 10$ kOe.

Sample (x)	M_i (emu g^{-1})	M_f (emu g^{-1})	T_C (K)	A (K^{-1})	B (emu/g.K)	$\|\Delta S_{max}\|$ (J/kgK)	RC (J/kg)
$x = 0$	71.9748	6.4565	255.3	0.0978	−0.159 23	4.52	45.2
$x = 0.02$	74.6291	6.4198	200.2	0.0770	−0.090 13	2.79	55.8
$x = 0.04$	71.7195	8.3353	166.5	0.0462	−0.135 51	1.58	69.5

The temperature dependence of the magnetization, $M(T)$, at $H = 100$ Oe for samples are show in figure 3(a). With increasing temperature, samples exhibit a FM-PM transition. T_C values determined from the flexion points in $M(T)$ curves are about 256, 198, and 166 K for $x = 0, 0.02$, and 0.04, respectively. Clearly, T_C value decreased monotonically with increasing Sn concentration. The decrease of T_C could be associated to a reduction of $\langle r_A \rangle$ value, which is a consequence of the replacing Sn with smaller radius into La/Ca-site. On the other hand, T_C value decreases because of the effect of the average ionic radius of A-site. Due to different ion sizes occupy at A-site (La/Ca/Sn-site) in perovskite structure, there is a size disorder between the ions. This disorder created a strong local stress in MnO_6 octahedral and also varying the Mn-O-Mn angles leading to the change in structural parameters and magnetic characters [28, 32].

Figure 3(b) shows $M(T)$ curves for samples measured at $H = 10$ kOe, where the solid lines are fitting curves of experimental data to a phenomenological model, which was suggested by Hamad [24, 25]. Detailed descriptions for this phenomenological model can be found elsewhere [24, 25, 32]. According to Hamad [24, 25], the temperature dependence of magnetization can be presented by:

$$M(T) = \left(\frac{M_i - M_f}{2}\right)[\tanh(A(T_C - T))] + BT + C, \quad (1)$$

with $A = \frac{2(B - S_C)}{(M_i - M_f)}$ and $C = \left(\frac{M_i + M_f}{2}\right) - BT_C$. Here, M_i and M_f are corresponding to the first and end values of magnetization at FM-PM phase transition; B and S_c are magnetization sensitivity dM/dT at FM state before transition and at T_C, respectively. Clearly, our experimental data (symbols) measured at $H = 10$ kOe for samples can be well fit by equation (1). Numerical calculation was made using the parameters listed in table 2.

To further understand the magnetic properties, we have recorded the isothermal magnetization $M(H)$ curves at temperatures around the FM-PM phase transition with a step of 2 K. Figures 3(c) and (d) show Arrott

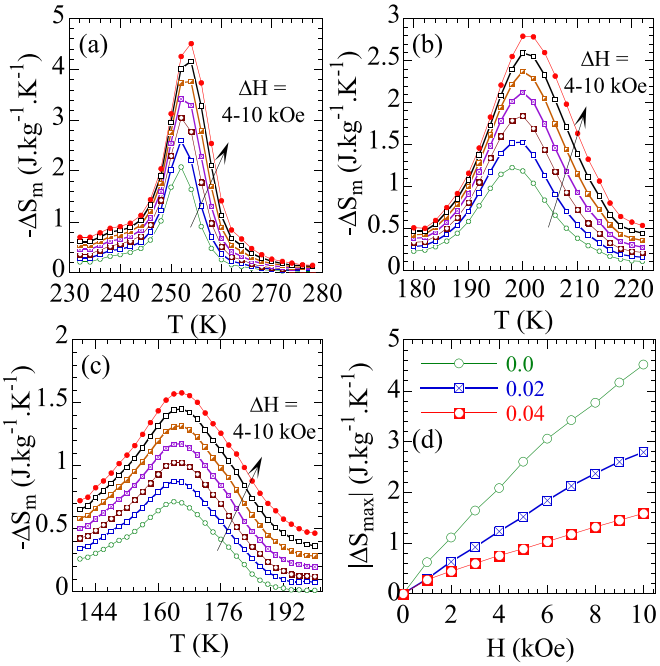

Figure 4. (a)–(c) $-\Delta S_m(T)$ curves for samples with $x = 0$, 0.02, and 0.04, respectively; (d) the variation of the $|\Delta S_{max}|$ values versus H.

plots, M^2 versus H/M, for two representative samples with $x = 0$ and 0.04, respectively (the tendency for $x = 0.02$ is similar with $x = 0.04$). As can be seen that the parts which do not linear in the low field range at the below and above T_C are driven toward two contrary dimensions, corresponding to the FM-PM phase division in the materials. Some H/M versus M^2 curves (coordinate axes are inverted to Arrott plots) of $x = 0$ with negative slopes indicate the FM-PM transition in this sample to be a FOPT, whereas the positive slopes for $x = 0.02$ and 0.04 correspond to the SOPT, according to Banerjee's criteria [21].

Based on the isothermal magnetization $M(H)$ data, the MCE for the samples are assessed via the ΔS_m by using the Maxwell relation [5, 14]

$$\Delta S_m(T, H) = \int_0^H \left(\frac{\partial M}{\partial T}\right)_H dH, \tag{2}$$

where H is the applied magnetic field magnitude. Figures 4(a)–(c) present $-\Delta S_m(T)$ curves calculated at different applied magnetic field change ($\Delta H = 4$–10 kOe with a step of 1 kOe). The $-\Delta S_m(T)$ curves which are a function of temperature exhibit the maxima ($|\Delta S_{max}|$) in the vicinity of T_C. These $|\Delta S_{max}|$ values increase with increasing applied magnetic field change, figure 4(d). Under an applied magnetic field change of 10 kOe, $|\Delta S_{max}|$ values are found to be 4.52, 2.79, and 1.58 J·kg^{-1}·K^{-1} for $x = 0$, 0.02, and 0.04. By comparison in the same field change, $|\Delta S_{max}|$ value obtained for $x = 0$ sample is higher than that of Gd metal ($|\Delta S_{max}| = 9.4$ J·kg^{-1}·K^{-1} under $\Delta H = 50$ kOe [33]). The high value of the magnetic entropy change in some manganites was also reported [9, 30, 28]. This is assigned to the presence of the double-exchange interaction and the spin lattice coupling [34]. For $x = 0.02$ and 0.04 samples, $|\Delta S_{max}|$ values obtained are quite high, and they are comparable to those obtained for other A-site doped manganites, such as $La_{0.7}Ca_{0.15}Sr_{0.15}MnO_3$ (1.57 J·kg^{-1}·K^{-1}, $\Delta H = 12$ kOe) [32], $La_{0.65}Ca_{0.3}Na_{0.05}MnO_3$ (3.0 J·kg^{-1}·K^{-1}, $\Delta H = 50$ kOe) [35], $La_{0.5}Ca_{0.4}Pb_{0.1}MnO_3$ (4.25 J·kg^{-1}·K^{-1}, $\Delta H = 50$ kOe) and $La_{0.5}Ca_{0.3}Pb_{0.2}MnO_3$ (4.2 J·kg^{-1}·K^{-1}, $\Delta H = 50$ kOe) [18], $(La_{0.8}Pr_{0.2})_{0.67}Ba_{0.33}MnO_3$ (2.25 J·kg^{-1}·K^{-1}, $\Delta H = 48$ kOe) [36]. Despite the value of $|\Delta S_{max}|$ is reduced with augmenting Sn-concentration, the $-\Delta S_m(T)$ curve is noticeably widened. With $\Delta H = 10$ kOe, the full width at half maximum (δT_{FWHM}) of $-\Delta S_m(T)$ curve can increase from 10 to 44 K when x increases from 0.0 to 0.04, corresponding to the refrigerant capacity $RC = |\Delta S_{max}| \times \delta T_{FWHM}$ values are about 45.2–69.5 J·kg^{-1}, see table 2. Interestingly, the value of $RC = 69.5$ J·kg^{-1} obtained for $x = 0.04$ sample is tantamount to that of Gd metal (63.4 J·kg^{-1} [37]). Therefore, this compound could be useful for the magnetic cooling technology.

According to [24, 25, 32], the magnetic entropy change (ΔS_m) and the adiabatic temperature change (ΔT_{ad}) of a magnetic system under adiabatic magnetic field change from 0 to H_{max} can be determined by using the equations

$$\Delta S_m = \left[\frac{-A(M_i - M_f)}{2} \mathrm{sech}^2(A(T_C - T)) + B\right] H_{max} \tag{3}$$

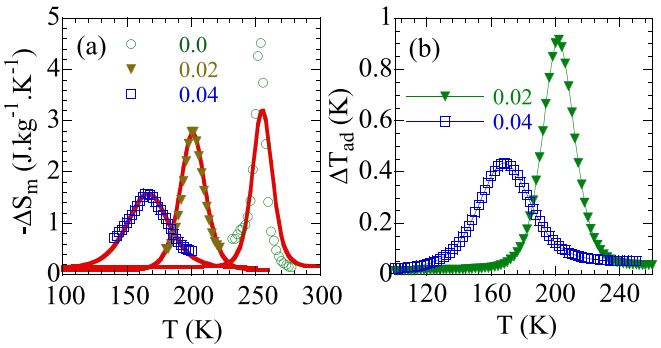

Figure 5. (a) $-\Delta S_m(T)$ curves for samples (symbols are experimental data, solid lines are results calculated from equation (3) and fitting parameters in table 2. (b) $\Delta T_{ad}(T)$ curves for two SOPT samples ($x = 0.02$ and 0.04) obtained by using equation (4) and fitting parameters in table 2.

$$\Delta T_{ad} = \frac{AT(M_i - M_f)}{2C_p}[\mathrm{sech}^2(A(T_C - T)) + B]H_{\max} \tag{4}$$

where C_p is the heat capacity. In this work, $C_p = 605$ J·kg^{-1}·K^{-1} has been used from [32]. Figure 5(a) shows the temperature dependence of magnetic entropy change of samples under an applied magnetic field change of 10 kOe. The symbols are the experimental data, the solid lines are results obtained by using equation (3) and model parameters in table 2. Clearly, the calculated data are in good agreement with the experimental data for $x = 0.02$ and 0.04. Whereas, there is a large deviation for $x = 0$. These may be related to the nature of FM-PM phase transition in the samples. It suggests that equation (3) is suitable for application on SOPT samples rather than on FOPT one. Thus, we have just used equation (4) and model parameters in table 2 to calculate the temperature dependence of adiabatic temperature change, $\Delta T_{ad}(T)$, for $x = 0.02$ and 0.04 as shown in figure 5(b). As a function of temperature, there is a peak around T_C on $\Delta T_{ad}(T)$ curve, which corresponds to the FM-PM phase transition. With 10 kOe, the maximum value of ΔT_{ad} is found to be 0.92 and 0.44 K for $x = 0.02$ and 0.04, respectively. These values are about 31.7 and 15.2% of those obtained from pure Gd metal (the maximum value of ΔT_{ad} for Gd is 5.8 K at 20 kOe [38]) if compared in the same applied magnetic field.

To learn about the nature of FM interactions in two SOPT samples ($x = 0.02$ and 0.04), we have investigated their critical behaviors. Firstly, we used four different models for trial exponents, including the mean field theory ($\beta = 0.5$ and $\gamma = 1.0$) [22], the 3D-Heisenberg model ($\beta = 0.365$ and $\gamma = 1.336$) [22], the 3D-Ising model ($\beta = 0.325$ and $\gamma = 1.241$) [22], and the tricritical mean field theory ($\beta = 0.25$ and $\gamma = 1.0$) [8] to build the $M^{1/\beta}$ versus $(H/M)^{1/\gamma}$ curves based on the $M(H)$ data in the vicinity of T_C for each sample (not shown). To select the best model, we have calculated the relative slope $S(T)/S(T_C)$, with $S(T)$ and $S(T_C)$ are slopes at temperatures T and T_C, respectively. It is known that if the values of β and γ are suitable, the $M^{1/\beta}$ versus $(H/M)^{1/\gamma}$ curves show a series of parallel lines, the relative slope should be kept to 1 independently of temperatures [39]. From figure 6(a) we can see that the values of β and γ with $x = 0.02$ can be best determined by the tricritical mean field theory. While, the critical properties for $x = 0.04$ can be described by the mean field theory. The set of $\beta = 0.25$, $\gamma = 1.0$ and $\beta = 0.5$, $\gamma = 1.0$ are thus selected as the trial values for our investigations into the critical behaviors of $x = 0.02$ and 0.04, respectively.

According to the Kouvel-Fisher method [23], the values of β, γ, and T_C could be determined from the relations:

$$\frac{M_S(T)}{dM_S(T)/dT} = \frac{T - T_C}{\beta}, \tag{5}$$

$$\frac{\chi_0^{-1}(T)}{d\chi_0^{-1}(T)/dT} = \frac{T - T_C}{\gamma} \tag{6}$$

Here, the $M_S(T)[dM_S(T)/dT]^{-1}$ and $\chi_0^{-1}(T)[d\chi_0^{-1}(T)/dT]^{-1}$ versus T plots would yield straight lines corresponding to $1/\beta$ and $1/\gamma$ slopes. These straight lines should extrapolate intercepts on the T axis equal to the T_C. Detailed descriptions for the Kouvel-Fisher method can be found elsewhere [23]. In this work, the values of $M_S(T)$ and $\chi_0^{-1}(T) = (H/M)(T)$ are determined from the intersections of the linear extrapolation line in high magnetic field areas with the $M^{1/\beta}$ and the $(H/M)^{1/\gamma}$ axes, and by using to equations (5) and (6), we get the new values of β, γ, and T_C, respectively. They are unbrokenly used for the next steps until achieving the durable β, γ, and T_C values. The Kouvel-Fisher plots for $x = 0.02$ and 0.04 with β and γ obtained from the final step are shown in figures 6(b) and (c), respectively. One can see that the value of T_C obtained for each sample from the Kouvel-Fisher method ($T_C \approx 197.3$ and 166.3 K for $x = 0.02$ and 0.04, respectively) is very close to that obtained from the $M(T)$ curve at figure 3(a). The critical exponent of δ can be got by fitting the critical isotherm

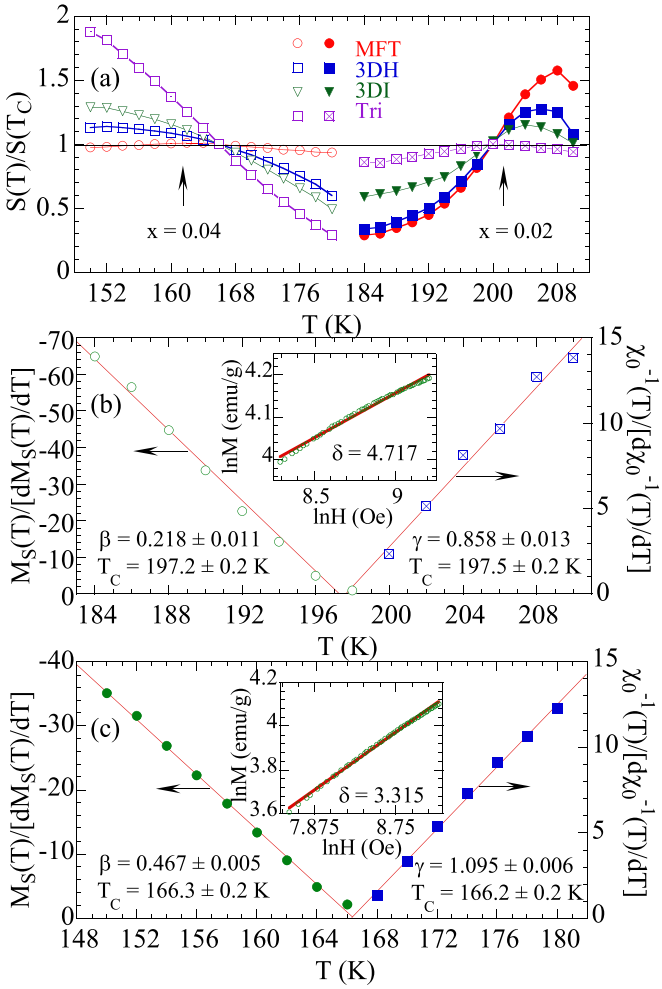

Figure 6. (a) Relative slope $S(T)/S(T_C)$ for two SOPT samples $x = 0.02$ and 0.04; abbreviations: MFT: mean field theory, 3DH; 3D-Heisenberg model, 3DI: 3D-Ising model, and Tri: Tricritical mean field theory. (b) and (c) the Kouvel-Fisher plots of $M_S(T)[dM_S(T)/dT]^{-1}$ and $\chi_0^{-1}(T)[d\chi_0^{-1}(T)/dT]^{-1}$ versus T are fitted to equations (5) and (6), respectively for $x = 0.02$ (b) and $x = 0.04$ (c).

$M(H, T_C)$ with below relation [22]

$$M = DH^{1/\delta} \tag{7}$$

where, D is the critical amplitude. In the insets of figures 6(b) and (c) shown that the δ value is 4.717 and 3.315 at $T = 198$ and 166 K for $x = 0.02$ and 0.04, respectively. In other words, critical exponents (β, γ, and δ) achieved from static scaling analysis are related by the Widom scaling relation $\delta = 1 + \gamma/\beta$ [22]. Plug the values of β and γ which are obtained from the Kouvel-Fisher method ($\beta = 0.218$, $\gamma = 0.858$ and $\beta = 0.467$, $\gamma = 1.095$ for $x = 0.02$ and 0.04, respectively) into this relation, we have calculated $\delta = 4.936$ and 3.345 for $x = 0.02$ and 0.04, respectively. These results are very close to those obtained by fitting the critical isotherm data $M(H, T \approx T_C)$ to equation (7). This proves that critical parameters β, γ, δ, and T_C obtained above are reliable. However, in the other way, checking the reliability of the obtained critical exponents and T_C values can be based on the scaling hypothesis [22]

$$M(H, \varepsilon) = \varepsilon^{\beta} f_{\pm}(H/\varepsilon^{(\beta+\gamma)}) \tag{8}$$

where $\varepsilon = (T\text{-}T_C)/T_C$ is the reduced temperature, $f_{\pm}$ are regular analytic functions for temperatures above and below T_C, respectively [22]. It insinuates that $M/|\varepsilon|^{\beta}$ as a function of $H/|\varepsilon|^{\beta+\gamma}$ falls into two universal curves, corresponding to $T > T_C$ and $T < T_C$ if determined values of critical exponents are correct. In this work, using the critical exponents and T_C values obtained above, the $M/|\varepsilon|^{\beta}$ versus $H/|\varepsilon|^{\beta+\gamma}$ data of $x = 0.02$ and 0.04 samples are plotted in the log-log scale as showed in figure 7. Interestingly, all experimental data of $M(H, T)$ fall on two universal branches for upper and lower T_C attesting that the values of β, γ and T_C determined above are trustworthy. However, the $M(H, T)$ data little deviates from the universal curves at the low fields ($H < 2$ kOe). It is attributed to the redistribution of magnetic domains where they are not entire in a straight line with the field.

Comparing our critical exponents determined and those of theoretical models (table 3) [8, 22], it can be clearly seen that $\beta = 0.218$, $\gamma = 0.858$, and $\delta = 4.717$ for $x = 0.02$ are quite near to those expected for the

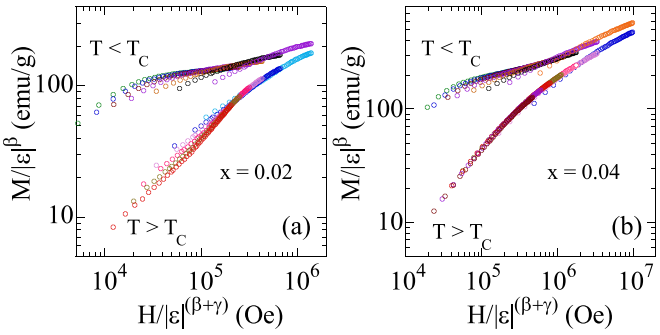

Figure 7. $M/|\varepsilon|^{\beta}$ versus $H/|\varepsilon|^{\beta+\gamma}$ curves on a log-log scale for $x = 0.02$ (a) and 0.04 (b).

Table 3. Critical parameters of typical models and some $La_{0.7}Ca_{0.3-x}A_xMnO_3$ manganites.

Model/Compound	T_C (K)	β	γ	δ	References
Mean field model	—	0.5	1.0	3.0	[22]
3D-Heisenberg model	—	0.365	1.386	4.80	[22]
3D-Ising model	—	0.325	1.241	4.82	[22]
Tricritical mean field model	—	0.25	1.0	5.0	[8]
$La_{0.7}Ca_{0.28}Sn_{0.02}MnO_3$	197	0.218 ± 0.011	0.858 ± 0.013	4.936	This work
$La_{0.7}Ca_{0.26}Sn_{0.04}MnO_3$	166	0.467 ± 0.005	1.095 ± 0.006	3.345	
$La_{0.7}Ca_{0.3}MnO_3$	222	0.14 ± 0.02	0.81 ± 0.03	1.22 ± 0.04	[40]
$La_{2/3}Ca_{0.75/3}Ba_{0.25/3}MnO_3$	277	0.356 ± 0.004	1.12 ± 0.02	4.1 ± 0.1	[41]
$La_{2/3}Ca_{0.5/3}Ba_{0.5/3}MnO_3$	306	0.402 ± 0.004	1.11 ± 0.02	3.7 ± 0.1	[41]
$La_{2/3}Ba_{1/3}MnO_3$	338	0.464 ± 0.003	1.29 ± 0.02	3.78 ± 0.01	[41]
$La_{0.7}Ca_{0.2}Sr_{0.1}MnO_3$	289	0.26 ± 0.01	1.06 ± 0.02	5.1 ± 0.2	[42]
$La_{0.7}Ca_{0.1}Sr_{0.2}MnO_3$	326	0.36 ± 0.01	1.22 ± 0.01	4.4 ± 0.2	[42]
$La_{0.7}Ca_{0.05}Sr_{0.25}MnO_3$	344	0.42 ± 0.02	1.14 ± 0.05	3.7 ± 0.2	[42]

tricritical mean field theory ($\beta = 0.25, \gamma = 1.0, \delta = 5.0$) [8]. It is suggested that $x = 0.02$ exhibiting tricriticality associated with the crossover of FOPT and SOPT, which is similar with that previous reported in $La_{0.7}Ca_{0.3}MnO_3$ ($\beta = 0.14, \gamma = 0.81$, and $\delta = 1.22$) [40] and $La_{0.7}Ca_{0.3}Mn_{1-x}Ni_xO_3$ ($\beta = 0.171$–0.262, $\gamma = 0.976$–0.979, and $\delta = 6.7$–4.7) [19]. Whereas, $\beta = 0.467, \gamma = 1.095, \delta = 3.315$ for $x = 0.04$ are very close to $\beta = 0.5, \gamma = 1.0, \delta = 3.0$ values belong to the mean field theory [22], indicating that this sample exists the long-range FM interactions. Clearly, there is a shifting tendency of the values of the critical exponents towards those of the mean field theory when increasing Sn-concentration in $La_{0.7}Ca_{0.3-x}Sn_xMnO_3$. It has been also observed on several La/Ca-site-doped manganites, such as $La_{0.7}Ca_{0.3-x}A_xMnO_3$ with A = Ba [41] and A = Sr [42]. Therefore, we believe that the substitution of Sn into La/Ca-site favors establishing FM long-range interactions in $La_{0.7}Ca_{0.3-x}Sn_xMnO_3$ compounds.

4. Conclusion

In summary, a detailed study on MCE and the critical behaviors of $La_{0.7}Ca_{0.3-x}Sn_xMnO_3$ compounds with $x = 0, 0.02$, and 0.04 around their T_C was carried out. The results demonstrated that a partial replacement of Ca by Sn in $La_{0.7}Ca_{0.3-x}Sn_xMnO_3$ plays an important role in decreasing T_C, $|\Delta S_{max}|$, and ΔT_{ad} values. Although the value of $|\Delta S_{max}|$ is reduced, the $-\Delta S_m(T)$ curves broaden remarkably and thus widen the working range, leading to an enhancement of the value of RC with Sn-doping increasing, making $La_{0.7}Ca_{0.3-x}Sn_xMnO_3$ compounds would be more useful in the magnetic refrigeration technology. Particularly, there is a FOPT to SOPT transformation when a partial of Ca is replaced by Sn in $La_{0.7}Ca_{0.3-x}Sn_xMnO_3$ with a threshold in the range of $x = 0$–0.02. The obtained critical exponents suggest an existence of the crossover of the FOPT and SOPT in $x = 0.02$. While, an existence of the long-range FM interactions in $x = 0.04$ has been observed. It means that the presence of Sn in $La_{0.7}Ca_{0.3-x}Sn_xMnO_3$ favors establishing SOPT with FM long-range interactions.

Acknowledgments

This article is partially supported by the Ministry of Science and Technology project (code B2019-TNA-01.VL), Thai Nguyen University of Science, Thai Nguyen University; and part of the funding from the grassroots project (CSL1.04.19), Institute of Materials Science, Vietnam Academy of Science and Technology; and part of Vietnam National Foundation for Science and Technology Development (NAFOSTED) under grant No. 103.02-2019.42.

ORCID iDs

Tran Dang Thanh https://orcid.org/0000-0002-8464-6743

References

[1] Dhal L, Andharia E, Shukla N, Kumary T G, Nigam A K, Malik S K, Santhosh P N and Nirmal R 2019 *J. Magn. Magn. Mater.* **474** 215
[2] Khlifi M, Dhahri J, Dhahri E and Hlil E K 2019 *J. Magn. Magn. Mater.* **480** 1
[3] Saravannan C, Thiyagarajan R, Kanjariya P V, Sivaprakash P, Bhalodia J A and Arumugam S 2019 *J. Magn. Magn. Mater.* **476** 35
[4] Ramirez A P 1997 *J. Phys. Condens. Matter* **9** 8171
[5] Phan M H and Yu S C 2007 *J. Magn. Magn. Mater.* **308** 325
[6] Arun B, Akshay V R, Chandrasekhar K D, Mutta G R and Vasundhara M 2019 *J. Magn. Magn. Mater.* **472** 74
[7] Yang H, Hua S, Pan M, Yu Y, Wu Q and Ge H 2019 *J. Supercond. Nov. Magn.* **32** 4021
[8] Kim D, Revaz B, Zink B L, Hellman F, Rhyne J J and Mitchell J F 2002 *Phys. Rev. Lett.* **89** 227202
[9] Hueso L E, Sande P, Miguens D R, Rivas J, Rivadulla F and Lopez-Quintela M A 2002 *J. Appl. Phys.* **91** 9943
[10] Zhang P, Lampen P, Phan T L, Yu S C, Thanh T D, Dan N H, Lam V D, Srikanth H and Phan M H 2013 *J. Magn. Magn. Mater.* **348** 146
[11] Lampen P, Bingham N S, Phan M H, Kim H, Osofsky M, Pique A, Phan T L, Yu S C and Srikanth H 2013 *Appl. Phys. Lett.* **102** 062414
[12] Kuz'min M D 2007 *Appl. Phys. Lett.* **90** 251916
[13] Phan T L, Thanh T D, Ho T A, Manh T V, Tran Q T, Lampen P, Phan M H and Yu S C 2014 *IEEE Trans. Magn.* **50** 2302604
[14] Taboada-Moreno A, Sánchez-De Jesús F, Pedro-García F, Cortés-Escobedo C A, Betancourt-Cantera J A, Ramírez-Cardona M and Bolarín-Miró A M 2020 *J. Magn. Magn. Mater.* **496** 165887
[15] Chaudhuri U, Chanda A and Mahendiran R 2020 *J. Magn. Magn. Mater.* **499** 166287
[16] Thanh T D, Lee T H, Phan T L, Tuan D A and Yu S C 2014 *J. Appl. Phys.* **115** 17C706
[17] Zeydi I, Zaidi A, Dhahri J and Hlil E K 2019 *J. Magn. Magn. Mater.* **471** 529
[18] Zarifi M, Kameli P, Raoufi T, Varzaneh A G, Salazar D, Nouraddini M I, Kotsedi L and Maaza M 2020 *J. Magn. Magn. Mater.* **494** 165734
[19] Phan T L, Tran Q T, Thanh P Q, Yen P D H, Thanh T D and Yu S C 2014 *Solid State Commun.* **184** 40
[20] Morán O, Gómez A, Supelano I, Parra C A and Izquierdo J L 2019 *J. Magn. Magn. Mater.* **477** 22
[21] Banerjee S K 1964 *Phys. Lett.* **12** 16
[22] Stanley H E 1971 *Introduction to Phase Transitions and Critical Phenomena* (London, U.K.: Oxford Univ. Press)
[23] Kouvel J S and Fisher M E 1964 *Phys. Rev.* **136** A1626
[24] Hamad M A 2013 *J. Therm. Anal. Calorim.* **111** 1251
[25] Hamad M A 2014 *J. Supercond. Nov. Magn.* **27** 269
[26] International Centre for Diffraction Data, PDF No. 01-089-8075 card 2020
[27] Dagotto E, Hotta T and Moreo A 2001 *Phys. Rep.* **344** 1
[28] Linh D C, Ha N T, Duc N H, Nam L H G, Bau L V, An N M, Yu S C and Thanh T D 2018 *Physica* B **532** 155
[29] Dhahri J, Dhahri A, Oumezzine M and Dhahri E 2008 *J. Magn. Magn. Mater.* **320** 2613
[30] Tka E, Cherif K and Dhahri J 2014 *Appl. Phys.* A **116** 1181
[31] Shannon R D 1976 Revised effective ionic radii and systematic studies of interatomic distances in halides and chalcogenides *Acta Crystallographica Section* A **32** 751
[32] Phong P T, Dang N V, Nam P H, Phong L T H, Manh D H, An N M and Lee I J 2016 *J. Alloys Compd.* **683** 67
[33] Pecharsky V K, Gschneidner K A and Tsokol A O 2005 *Rep. Prog. Phys.* **68** 1479
[34] Asamitsu A, Moritomo Y, Tomloka Y, Arima T and Tokura Y 1995 *Nature* **373** 407
[35] Koubaa M, Koubaa W C and Cheikhrouhou A 2009 *Phys. Procedia* **2** 997
[36] Cetin S K 2020 *J. Supercond. Nov. Magn.* **33** 683
[37] Wang D, Han Z, Cao Q, Huang S, Zhang J and Du Y 2005 *J. Alloys Compd.* **396** 22
[38] Yu Dan'kov S, Tishin A M, Pecharsky V K and Gschneidner K A Jr 1998 *Phys. Rev.* B **57** 3478
[39] Fan J, Ling L, Hong B, Zhang L, Pi L and Zhang Y 2010 *Phys. Rev.* B **81** 144426
[40] Shin H S, Lee J E, Nam Y S, Ju H L and Park C W 2001 *Solid State Commun.* **118** 377
[41] Phan T L, Zhang P, Grinting D, Lam V D, Tuan D A and Yu S C 2012 *IEEE Trans. Magn.* **48** 4018
[42] Phan M H, Franco V, Bingham N S, Srikanth H, Hur N H and Yu S C 2010 *J. Alloys Compd.* **508** 238